Further accuracy and convergence results on the modeling of flows down inclined planes by weighted-residual approximations

Christian Ruyer-Quil, Paul Manneville

Further accuracy and convergence results on the modeling of flows down inclined planes by weighted-residual approximations

Christian Ruyer-Quil and Paul Manneville

Citation: Physics of Fluids (1994-present) **14**, 170 (2002); doi: 10.1063/1.1426103
View online: http://dx.doi.org/10.1063/1.1426103
View Table of Contents: http://scitation.aip.org/content/aip/journal/pof2/14/1?ver=pdfcov
Published by the AIP Publishing

Further accuracy and convergence results on the modeling of flows down inclined planes by weighted-residual approximations

Christian Ruyer-Quil[a] and Paul Manneville
Laboratoire d'Hydrodynamique–UMR CNRS 7646, École polytechnique, 91128 Palaiseau, France

(Received 5 October 2000; accepted 2 October 2001)

We study the reliability of two-dimensional models of film flows down inclined planes obtained by us [Ruyer-Quil and Manneville, Eur. Phys. J. B **15**, 357 (2000)] using weighted-residual methods combined with a standard long-wavelength expansion. Such models typically involve the local thickness h of the film, the local flow rate q, and possibly other local quantities averaged over the thickness, thus eliminating the cross-stream degrees of freedom. At the linear stage, the predicted properties of the wave packets are in excellent agreement with exact results obtained by Brevdo *et al.* [J. Fluid Mech. **396**, 37 (1999)]. The nonlinear development of waves is also satisfactorily recovered as evidenced by comparisons with laboratory experiments by Liu *et al.* [Phys. Fluids **7**, 55 (1995)] and with numerical simulations by Ramaswamy *et al.* [J. Fluid Mech. **325**, 163 (1996)]. Within the modeling strategy based on a polynomial expansion of the velocity field, optimal models have been shown to exist at a given order in the long-wavelength expansion. Convergence towards the optimum is studied as the order of the weighted-residual approximation is increased. Our models accurately and economically predict linear and nonlinear properties of film flows up to relatively high Reynolds numbers, thus offering valuable theoretical and applied study perspectives. © *2002 American Institute of Physics.* [DOI: 10.1063/1.1426103]

I. INTRODUCTION

The long wavelength interfacial instability modes of viscous film flows down inclined planes have attracted much interest since the pioneering work of Kapitza.[1] In practice, at low to moderate Reynolds numbers the space–time evolution of films are slow and internal fluctuations remain mostly enslaved to the local film thickness h so that the initially three-dimensional free-boundary problem can be dramatically simplified by the elimination of the cross-stream (y) dependence of the velocity field leading to a simpler two-dimensional, streamwise (x) and spanwise (z), problem,[2] and even to a one-dimensional streamwise problem when taking into account Squire's theorem,[3] as long as secondary instabilities do not introduce spanwise modulations, which shall be assumed in all what follows. These features call for the derivation of models with reduced dimensionality able to deal with the dynamics of the film at a quantitative level.

The cleanest modeling strategy is clearly by defining a *film parameter* $\epsilon \sim |\partial_x h|/h$ and performing an expansion in terms of ϵ, then truncating it at some level. All the flow variables are then asymptotically enslaved to the evolution of the film thickness $h(x,t)$, which yields a one-equation description of the film's dynamics in the form $\partial_t h = G(h^n, \partial_{x^m} h,)$, the prototype of which is the Benney equation[4]

$$\partial_t h + h^2 \partial_x h + \tfrac{1}{3}\partial_x[(\tfrac{2}{5}h^6 - Bh^3)\partial_x h + \Gamma h^3 \partial_{xxx} h] = 0. \quad (1)$$

Here, space–time scales are defined using ν (kinematic viscosity) and $g \sin\beta$ (streamwise gravity acceleration), where β is the angle made by the plane with the horizontal ($B = \cot\beta$). The Kapitza number $\Gamma = \gamma/[\rho \nu^{4/3}(g \sin\beta)^{1/3}]$ compares surface tension γ to viscosity and gravity. In this formulation, the control parameter is the height h_N of the film in its basic state, which corresponds to a flow with a time-independent spatially uniform thickness and a semiparabolic velocity profile called the Nusselt solution. A perhaps more traditional presentation makes use of a Reynolds number based on the film thickness and the flow speed at the interface, and a Weber number to measure the strength of surface tension effects. These two numbers are defined in terms of h_N and Γ as $R = \frac{1}{2}h_N^3$ and $W = \Gamma/h_N^2$. The resulting Benney equation has of course strictly the same structure as (1). The advantage of using the Kapitza number, defined only in terms of the fluid properties and the geometry of the experiment, is somewhat compensated by the fact that, from a physical point of view, the effects of surface tension have to be compared to inertia effects, which the Weber number does appropriately.

At any rate, Eq. (1) cannot be a good model of unstable film with space–time modulated thickness since, unfortunately not far beyond threshold, its solutions experience finite-time blow up[5] despite the regularizing effects of surface tension that enter the problem *via* the term $\frac{1}{3}\Gamma \partial_x(h^3 \partial_{xxx} h)$, active at lowest order owing to the implicit assumption $\Gamma \epsilon^2 = \mathcal{O}(1)$. Truncating the ϵ expansion at higher orders does not improve the situation but this behavior can be cured by a Padé resummation technique.[6] The procedure is, however, not fully satisfactory since it leads to underestimating the characteristics (amplitude and speed) of the solitary wave solutions (Ref. 7, see Fig. 2). Therefore, it

[a]Address: Laboratoire FAST–UMR CNRS 7608, Campus universitaire, 91405 Orsay, France.

does not seem possible to describe the dynamics of the film sufficiently far from threshold in terms of a single evolution equation for h and one is led to consider systems of several equations for the film thickness h and other average quantities, the most obvious one being the local flow rate $q(x,t) = \int_0^h u(y,x,t)dy$.

By assuming a streamwise parabolic velocity profile $u \propto \bar{y} - \frac{1}{2}\bar{y}^2$ where $\bar{y} = y/h$, h being a function of time and space, and integrating the streamwise momentum equation along the y direction (Polhausen–von-Kármán averaging method also called the *integral method*) Shkadov[8] obtained for the local flow rate q the following equation:

$$\partial_t q = h - Bh\partial_x h + \Gamma h \partial_{xxx} h - 3\frac{q}{h^2} - \frac{12}{5}\frac{q}{h}\partial_x q + \frac{6}{5}\frac{q^2}{h^2}\partial_x h\,, \tag{2}$$

which, when completed by the kinematic condition at the interface written in conservative form as

$$\partial_t h + \partial_x q = 0, \tag{3}$$

where q is the local flow rate introduced above, forms the first closed two-equation model of film flow, often called the integral boundary layer (IBL) model.

The main limitation of this model can be noticed just by performing a gradient expansion of the flow rate $q = q^{(0)} + q^{(1)}\cdots$, then truncating it at first order and solving it for h. This yields a Benney-like equation but with a coefficient 1/3 for the h^6-term instead of the exact factor 2/5 in (1). The first visible consequence of this difference is an erroneous estimation of the linear instability threshold $q_c^{(\mathrm{IBL})} = B$ instead of $q_c^{(\mathrm{th})} = \frac{5}{6}B$, as obtained from both (1) or a direct Orr–Sommerfeld stability analysis. In the case of a vertical plane, $\beta = \pi/2$ hence $B = 0$, the model trivially predicts the correct result that the flow is unstable at all Reynolds numbers but the limitation immediately shows up at the nonlinear stage. It has been attempted to cure this deficiency by adding higher-order terms[9] or surface-tension corrections[10] but the incorrect IBL threshold prediction was reobtained. This failure can be traced back to the lack of flexibility of the assumed velocity profile, either the simple parabolic profile or some other fixed profile function of y/h (called *similar* by reference to the theory of boundary layers), while corrections to it are known to exist, already at first order, from the long-wavelength expansion.

In Sec. II, we first recall the methodology and main results of our systematic modeling attempt[7] using a weighted-residual method[11] based on a polynomial expansion of the velocity profile combined to the classical long-wavelength expansion. Optimal modeling consistent at first (second) order in the long-wavelength expansion was further shown to involve one (three) field(s) in addition to the thickness h. A simplified second-order model obtained by adiabatic elimination of two of the three fields of the full optimal second-order model was suggested to be a valuable intermediate with much less complexity and still sufficient accuracy. In Sec. III, we prove that the flexibility introduced in the velocity profile makes our modeling reliable in a wide range of Reynolds numbers above threshold by comparing quantitatively the results of a conventional linear stability analysis, here amounting to a simple study of an explicit, polynomial, dispersion relation, with the output of the exact analysis performed by Brevdo *et al.*[12] In this respect, the comparison of results for the full and simplified second-order models turns out to be specially instructive. Section IV is devoted to an illustration of the nonlinear dynamics of the simplified second-order model mimicking an unstable film with the same characteristics as those used by Liu and Gollub in their experiments[13] or by Ramaswamy *et al.* in their simulations,[14] and showing that the quantitative agreement obtained at the linear level is also achieved at the nonlinear level. The convergence of the weighted-residual techniques toward optimal models as the number of basis functions is increased is also a subject of interest. We examine this problem in Sec. V where, for the sake of simplicity, we restrict ourselves to the case of the simplified second-order for which we need to study only one equation for one single supplementary field. Taking advantage of this situation we compare the efficiency of several weighting strategies, showing that the best technique seems to be the classical Galerkin approach in which weight functions are taken in the same set as the basis functions. Some concluding remarks are presented in Sec. VI.

II. THE POLYNOMIAL EXPANSION APPROACH

The Polhausen–von-Kármán averaging method can be viewed as a special case of more general methods of weighted residuals.[11] Let the problem at hand be formally written as $\mathcal{E}(\mathcal{U}) = 0$ for some set of field variables $\mathcal{U}$. The solution to it is searched for in the form of a series expansion $\mathcal{U} = \Sigma_{j=0}^{j_{\max}} a_j f_j$, where the f_j, $j = 0,...,j_{\max}$, are test functions and the a_j their amplitudes. Weight functions w_j, $j = 0,...,j_{\max}$, are next chosen as ingredients of a projection rule defining the residuals: $\mathcal{R}_{j'} = \langle w_{j'} | \mathcal{E}(\Sigma a_j f_j)\rangle$, $j' = 0,...,j_{\max}$. Canceling the residuals $\mathcal{R}_{j'}$ thus yields a system to be solved for the amplitudes a_j. The search for an accurate solution is achieved by increasing the truncation order $j_{\max}$, whereas modeling relies mostly on low-order approximations. Many different methods follow this general scheme but differ by the specification of the projection rule.

In the present problem, the slow space–time dynamics of the film suggests a natural separation of variables with the (x,t) dependence included in the amplitudes a_j and the cross-stream dependence accounted for by test functions in terms of the reduced variable $\bar{y} = y/h$. The use of $\bar{y}$, instead of simply y, accounts from the start for the fact that the flow profile is locally enslaved to the thickness h, trivially for the flat film Nusselt solution, but also less trivially through its space–time derivatives when the interface height is no longer uniform, as becomes obvious from the long-wavelength expansion.[4,15,16] Indeed, within this expansion the streamwise velocity field can be written in the form $u = \Sigma \epsilon^n G_{n,j}(h^k, \partial_{x^l} h)\mathsf{P}_{n,j}(\bar{y})$, where $G_{n,j}$ are functions of h and its gradients and $\mathsf{P}_{n,j}$ are polynomials.

We begin the review of our previous work[7,16] by writing down the equations corresponding to the two-dimensional

(x,y) film flow problem at first order in the gradient expansion, which parallels the boundary layer theory leading to the Prandtl equation. From the continuity condition

$$\partial_x u + \partial_y v = 0, \tag{4}$$

where $\partial_x u$ is of order ϵ, it appears that the cross-stream velocity v is also of order ϵ. Lowest order terms in the cross-stream momentum equation (i.e., for v) are then of order ϵ and inertial terms $\partial_t v + u\partial_x v + v\partial_y v$, of order ϵ^2, can be dropped to get the pressure at order ϵ by integrating the remains of this equation over y (see Ref. 16 for details). The streamwise pressure gradient is then obtained as $\partial_x p = B\partial_x h - \Gamma\partial_{xxx} h$ which, upon insertion in the streamwise momentum equation (i.e., for u), leads to

$$\partial_{yy} u + 1 = \partial_t u + u\partial_x u + v\partial_y u + B\partial_x h - \Gamma\partial_{xxx} h, \tag{5}$$

where it is immediately checked that every term on the right hand side is of order ϵ under the assumption $\Gamma\epsilon^2 = \mathcal{O}(1)$. As to the boundary conditions, a classical no-slip condition holds at the solid plane $y=0$, hence

$$u|_0 = 0, \tag{6a}$$

$$v|_0 = 0, \tag{6b}$$

whereas at the interface $y=h$ one gets

$$v|_h = \partial_t h + u|_h \partial_x h, \tag{7a}$$

$$\partial_y u|_h = 0, \tag{7b}$$

where (7a) accounts for the kinematics of the interface and (7b) for the continuity of the tangential stress at the free surface. This set of equations is completed by (4) which helps us determine v from u when needed, and by (3) where q is the local flow rate introduced earlier and which replaces (7a) using (4) once integrated over y.

Our specific modeling strategy starts with an expansion of the velocity field $u = \Sigma a_j(x,t) f_j(\overline{y})$ in terms of polynomial test functions. This choice was made upon four considerations: (i) The flat film solution has a parabolic velocity profile; (ii) polynomials form a closed set with respect to products and differentiations; (iii) corrections to the parabolic profile appearing in the Benney expansion are precisely polynomials; (iv) this choice allows simple algebraic manipulations. Once the test functions f_j and the weight functions $w_j(\overline{y})$ have been defined, the application of the weighted-residual technique is straightforward. The system of equations to solve for the amplitudes a_j of the streamwise velocity field u are provided by the boundary conditions (6)–(7) and the projection of the momentum equation (5) defined by the weighting rules. The effectiveness of several such rules is considered later in Sec. V.

For convenience, the first polynomial f_0 is chosen to be the semi-parabolic profile corresponding to the flat film so that $f_0 \equiv \overline{y} - \frac{1}{2}\overline{y^2}$. Now, the technically important fact is that, when the film is flat, one has $a_j \equiv 0$, for all $j \geqslant 1$, whereas when it is (slowly) modulated, these coefficients are at least of the order of the space and time gradients of h. In the same time, a_0 is a zeroth order quantity that enters the expansion together with its gradients. Therefore, truncating the problem to solve at order ϵ, the derivatives of the fields a_j, $j \geqslant 1$, are quantities of higher order that can be dropped in the evaluation of the residuals. The cancellation of $j_{\max}+1$ residuals for $j_{\max}+1$ test functions then leads to a system of equations where the a_j, $j \geqslant 1$, enter linearly and undifferentiated, while a_0 appear either linearly or quadratically [from $u\partial_x u + v\partial_y u$ in Eq. (5)] together with its derivatives with respect to x or t. The system governing all the amplitudes a_j except a_0, can then be written as

$$\sum_{j'=1}^{j_{\max}} \alpha_{jj'} a_{j'} = \beta_j(h, a_0, \partial_t h, \partial_x h, \partial_t a_0, \partial_x a_0),$$

$$j = 1, \ldots, j_{\max},$$

where the matrix $[\alpha_{jj'}]$ is invertible. Solving for the a_j, $j \geqslant 1$, and inserting their expression in the residual for a_0 yields a nonlinear equation linking a_0 to its gradients and those of h (see Ref. 7 for details).

However, a_0 has no physical meaning and it is preferable to turn to the local flow rate $q(x,t)$ that is directly involved in the mass conservation equation (3). From its definition $q = \Sigma_{i=0}^{j_{\max}} h\, a_i \int_0^1 f_i(\overline{y})\, d\overline{y}$, one can exchange a_0 for q using (3) and taking into account the expressions of the a_j, $j \geqslant 1$. We obtain

$$\partial_t q = \frac{5}{6}(h - Bh\partial_x h + \Gamma h \partial_{xxx} h) - \frac{5}{2}\frac{q}{h^2} - \frac{17}{7}\frac{q}{h}\partial_x q + \frac{9}{7}\frac{q^2}{h^2}\partial_x h, \tag{8}$$

Eq. (3) closing the system.

The complete derivation[7] shows that the corrections to the parabolic profile are strictly slaved to h, q, and their gradients and, by simple power counts, that polynomials up to degree 6 have to be included in the expansion in order to obtain a consistent account of the film's dynamics at order ϵ, starting with a correct determination of the linear instability threshold.[17] Model [(3), (8)] has been termed *optimal* at first order in the sense that the polynomial velocity field reconstructed from the coefficients a_j fulfills (5) exactly and not only in average, so that the Benney equation is recovered through the appropriate expansion. Accordingly, any other model based on weighted residuals and polynomial test functions will thus converge to it when the size of the basis is increased, as shown in Sec. V.

In order to be consistent at order ϵ^2, Eq. (5) and boundary condition (7b) have to be completed to read

$$\partial_{yy} u + 1 = \partial_t u + u\partial_x u + v\partial_y u - 2\partial_{xx} u - \partial_x[\partial_x u|_h] + B\partial_x h - \Gamma\partial_{xxx} h, \tag{9}$$

$$\partial_y u|_h = 4\partial_x h \partial_x u|_h - \partial_x v|_h. \tag{10}$$

All supplementary terms originate from viscous dissipation effects whereas Eqs. (3), (4), (6), and (7a) remain unchanged. The derivation of the model becomes much more cumbersome because corrections to the parabolic profile are no longer enslaved to the dynamics of a_0 and become free variables.[7] Consistency requires the introduction of polyno-

mials up to degree 14 because the complete expression of the velocity field at order ϵ is a polynomial of degree 6. Out of the corresponding 15 amplitudes, only three are independent variables. One is a_0, associated to the semiparabolic profile as previously, the two others are specific polynomial corrections to the basic velocity profile of degree 4 and 6, respectively. They were slaved to a_0 at order ϵ but their space–time derivatives contribute at order ϵ^2. The result is a system of three equations for three unknowns, q and two supplementary variables, called s_1 and s_2, measuring the relevant corrections to the flow rate

$$\partial_t q = \frac{27}{28}h - \frac{81}{28}\frac{q}{h^2} - 33\frac{s_1}{h^2} - \frac{3069}{28}\frac{s_2}{h^2} - \frac{12}{5}\frac{q s_1 \partial_x h}{h^2} - \frac{126}{65}\frac{q s_2 \partial_x h}{h^2} + \frac{12}{5}\frac{s_1 \partial_x q}{h} + \frac{171}{65}\frac{s_2 \partial_x q}{h} + \frac{12}{5}\frac{q \partial_x s_1}{h} + \frac{1017}{455}\frac{q \partial_x s_2}{h} + \frac{6}{5}\frac{q^2 \partial_x h}{h^2} - \frac{12}{5}\frac{q \partial_x q}{h} + \frac{5025}{896}\frac{q(\partial_x h)^2}{h^2} - \frac{5055}{896}\frac{\partial_x q \partial_x h}{h} - \frac{10851}{1792}\frac{q \partial_{xx} h}{h} + \frac{2027}{448}\partial_{xx} q - \frac{27}{28}Bh\,\partial_x h + \frac{27}{28}\Gamma h \partial_{xxx} h\,, \tag{11}$$

$$\partial_t s_1 = \frac{1}{10}h - \frac{3}{10}\frac{q}{h^2} - \frac{3}{35}\frac{q^2 \partial_x h}{h^2} - \frac{126}{5}\frac{s_1}{h^2} - \frac{126}{5}\frac{s_2}{h^2} + \frac{1}{35}\frac{q \partial_x q}{h} + \frac{108}{55}\frac{q s_1 \partial_x h}{h^2} - \frac{5022}{5005}\frac{q s_2 \partial_x h}{h^2} - \frac{103}{55}\frac{s_1 \partial_x q}{h} + \frac{9657}{5005}\frac{s_2 \partial_x q}{h} - \frac{39}{55}\frac{q \partial_x s_1}{h} + \frac{10557}{10010}\frac{q \partial_x s_2}{h} + \frac{93}{40}\frac{q(\partial_x h)^2}{h^2} - \frac{69}{40}\frac{\partial_x h \partial_x q}{h} + \frac{21}{80}\frac{q \partial_{xx} h}{h} - \frac{9}{40}\partial_{xx} q - \frac{1}{10}Bh\partial_x h + \frac{1}{10}\Gamma h \partial_{xxx} h\,, \tag{12}$$

$$\partial_t s_2 = \frac{13}{420}h - \frac{13}{140}\frac{q}{h^2} - \frac{39}{5}\frac{s_1}{h^2} - \frac{11817}{140}\frac{s_2}{h^2} - \frac{4}{11}\frac{q s_1 \partial_x h}{h^2} + \frac{18}{11}\frac{q s_2 \partial_x h}{h^2} - \frac{2}{33}\frac{s_1 \partial_x q}{h} - \frac{19}{11}\frac{s_2 \partial_x q}{h} + \frac{6}{55}\frac{q \partial_x s_1}{h} - \frac{288}{385}\frac{q \partial_x s_2}{h} - \frac{3211}{4480}\frac{q(\partial_x h)^2}{h^2} + \frac{2613}{4480}\frac{\partial_x h \partial_x q}{h} - \frac{2847}{8960}\frac{q \partial_{xx} h}{h} + \frac{559}{2240}\partial_{xx} q - \frac{13}{420}Bh\partial_x h + \frac{13}{420}\Gamma h \partial_{xxx} h\,. \tag{13}$$

As before, this set of equations is closed by (3).

The complete expression of the optimal second-order model [(3), (11)–(13)] is hardly tractable and a simplified version would be welcome. As a matter of fact, standard linear stability analysis shows that the relaxation times of s_1 and s_2 are much shorter than those of q so that their adiabatic elimination seems legitimate. Admitting that, apart from corrections of order higher than ϵ^2, their values are, at every instant, enforced by the instantaneous local value of fields h and q we obtain the approximate second-order model

$$\partial_t q = \frac{5}{6}h - \frac{5}{2}\frac{q}{h^2} - \frac{17}{7}\frac{q}{h}\partial_x q + \left(\frac{9}{7}\frac{q^2}{h^2} - \frac{5}{6}Bh\right)\partial_x h + 4\frac{q}{h^2}(\partial_x h)^2 - \frac{9}{2h}\partial_x q \partial_x h - 6\frac{q}{h}\partial_{xx} h + \frac{9}{2}\partial_{xx} q + \frac{5}{6}\Gamma h \partial_{xxx} h\,. \tag{14}$$

Comparing this equation to (8), one can trace back the origin of the new terms, all on the second line, to the effects of viscous dissipation at second order, i.e., from the terms $-2\partial_{xx}u - \partial(\partial_x u|_h)$ in the momentum equation (9) and $4\partial_x h\,\partial_x u|_h - \partial_x v|_h$ in the boundary condition (10). As a matter of fact, their presence in any second-order two-equation model involving h and q and their gradients is easily understood from the fact that $\partial_{xx} q$, $\partial_x q(\partial_x h/h)$, $q(\partial_x h/h)^2$ and $q(\partial_{xx} h/h)$ are the only homogeneous terms, linear in q and formally of second order in ∂_x. This will be illustrated later in Sec. V where, according to the weighting strategy, they will appear in the models derived there with different coefficients which will be shown to converge to their values in (14) as the approximation level is increased. A more accurate two-equation model should also contain second-order terms of inertial origin, thus formally quadratic in q, but it will be seen in the two next sections that the drastic simplification made to obtain (14) is already effective. Model [(3), (14)] will accordingly be called the "simplified second order model" in all what follows.

Any evaluation of the range of validity of models based on the long-wavelength expansion is difficult owing to supplementary assumptions which link the amplitude of the gradients to the intensity of the regularizing effects of surface tension through some least degeneracy principle, $\Gamma\epsilon^2 = \mathcal{O}(1)$ for first-order models and $\Gamma\epsilon = \mathcal{O}(1)$ at second order. When Γ is large, allowed gradients are small and a truncation of the ϵ expansion at a low order is expected to give reasonable results for waves with lengths large when compared to the basic (Nusselt) film thickness, but a direct check of the accuracy would be welcome. To this aim, linear stability predictions from our three models, optimal first-order, optimal second-order, approximate second-order, are quantitatively confronted to the exact results of Brevdo *et al.*[12] in the next section. The development of forced waves trains obtained by numerical simulation of our models is then compared to observations by Liu *et al.*[18] and direct numerical simulations by Ramaswamy *et al.*[14]

III. LINEAR STABILITY RESULTS

Following common practice, we first discuss the film flow stability in terms of the dispersion relation linking, in the fully complex case, the wave number $k=k_r+ik_i$ and the pulsation $\omega=\omega_r+i\omega_i$ of infinitesimal perturbations to the Nusselt flat film solution, $h\equiv h_N$, i.e., varying as $\exp[i(kx-\omega t)]$. Temporally growing (decaying) modes thus correspond to $\omega_i>0$ ($\omega_i<0$), downstream (upstream) growing modes to $k_i<0$ ($k_i>0$), and neutral waves to $k_i=\omega_i=0$. Linearization of model [(3), (8)] around $h=h_N$ and $q=\frac{1}{3}h_N^3$ yields

$$i\frac{5}{2h_N^2}\omega+\omega^2+\left(-i\frac{5}{2}-\frac{17h_N^2}{21}\omega\right)k+\frac{5}{2}h_N\left(-\frac{B}{3}+\frac{2}{35}h_N^3\right)k^2-\frac{5}{6}\Gamma h_N k^4=0. \tag{15}$$

In view of the comparisons to be made, it is more convenient to turn to a scaling based on the film thickness h_N and the flow velocity at the interface u_N, hence the transformation $k\mapsto k/h_N$ and $\omega\mapsto h_N\omega/2$ so that (15) now reads

$$i\tfrac{5}{2}\omega+R\omega^2+(-5i-\tfrac{34}{21}R\omega)k+(-\tfrac{5}{3}B+\tfrac{4}{7}R)k^2-\tfrac{5}{3}Wk^4=0, \tag{16}$$

in which definitions $R=\frac{1}{2}h_N^3$ and $W=\Gamma/h_N^2$ have been introduced. Canceling the imaginary part of the dispersion relation for real k yields the marginal condition (subscript "m") $\omega_m=2k_m$, hence a phase velocity $c=2$. The real part in turn yields

$$k_m=\sqrt{\frac{1}{W}\left(\frac{4}{5}R-B\right)}, \tag{17}$$

which is nothing but what can be predicted from the Benney equation, exact for $R\approx R_c=\frac{5}{4}B$ only. In the case of the simplified second-order model [(3), (14)], using the same scalings, the dispersion relation reads

$$i\tfrac{5}{2}\omega+R\omega^2+(-5i-\tfrac{34}{21}R\omega)k+(-\tfrac{5}{3}B+\tfrac{4}{7}R+i\tfrac{9}{2}\omega)k^2-4ik^3-\tfrac{5}{3}Wk^4=0, \tag{18}$$

which differs from (16) by two terms accounting for the contribution of the viscous dispersive effects. Finally, linearization of the full second-order model [(3), (11)–(13)] leads to

$$\mathsf{A}+\mathsf{B}k+\mathsf{C}k^2+\mathsf{D}k^3+\mathsf{E}k^4+\mathsf{F}k^5+\mathsf{G}k^6=0, \tag{19}$$

in which

$$\mathsf{A}=i\frac{5}{2}\omega+\frac{15}{13}R\omega^2-\frac{25}{429}iR^2\omega^3-\frac{2}{3861}R^3\omega^4,$$

$$\mathsf{B}=-5\,i-\frac{290}{143}R\omega+\frac{490}{3861}iR^2\omega^2+\frac{4}{3003}R^3\omega^3,$$

$$\mathsf{C}=-\frac{5}{3}B+\frac{332}{429}R+\omega\left(\frac{9}{2}i+\frac{4}{39}iBR-\frac{29\,360}{351\,351}iR^2\right)+\omega^2\left(\frac{359}{1456}R+\frac{1}{1001}BR^2-\frac{136}{117\,117}R^3\right)-\frac{2027}{864\,864}iR^2\omega^3,$$

$$\mathsf{D}=-4\,i-\frac{608}{9009}iBR+\frac{608}{39039}iR^2+\omega\left(-\frac{12\,205}{36\,036}R-\frac{32}{27\,027}BR^2+\frac{1472}{3\,864\,861}R^3\right)+\frac{3439}{786\,240}iR^2\omega^2,$$

$$\mathsf{E}=\frac{10\,331}{96\,096}R+\frac{592}{1\,756\,755}BR^2-\frac{128}{3\,864\,861}R^3-\frac{5}{3}W+\omega\left(-\frac{4591}{1\,756\,755}iR^2+\frac{4}{39}iWR\right)+\frac{1}{1001}WR^2\omega^2,$$

$$\mathsf{F}=\frac{197}{390\,390}iR^2-\frac{608}{9009}iWR-\frac{32}{27\,027}WR^2\omega,$$

$$\mathsf{G}=\frac{592}{1\,756\,755}WR^2.$$

A comparison of (18) and (19) shows that all the terms in (18) are also in (19). The terms independent of R are merely identical. Those linear in R are recovered with slightly different coefficients and all other terms in (19) have R at some power $\geqslant 1$ in factor, which accounts for the fact that the second-order model includes inertial corrections not present in the simplified models.

Controlled experiments devoted to the detection of marginal conditions are generally performed by forcing the film at the inlet, either its thickness or its flow rate, at some frequency and by detecting the cut-off frequency f_c beyond which the film remains flat. Frequency f_c is thus determined from the dispersion relation by imposing that the spatial growth rate, i.e., the imaginary part k_i of the complex wave vector k, of a mode with given real pulsation $\omega_r=\omega$ just cancels, which yields the Reynolds number as a function of the frequency $\omega/2\pi=f_c$, together with the marginal wave vector k_m from which the phase velocity of the waves can be derived. The curves obtained from the simplified and full second-order dispersion relations (18) and (19), displayed in Fig. 1 as a thin and thick solid line respectively, compare equally well with the experimental data by Liu *et al.*[18] within error bars. The increasing discrepancy between the first-order prediction (17) corresponding to the dashed line in Fig. 1—Shkadov's model (dot–dashed line) doing even worse in predicting an erroneous threshold—and the experiment can therefore be attributed mainly to the neglect of the streamwise viscous dissipation and the subsequent phase velocity

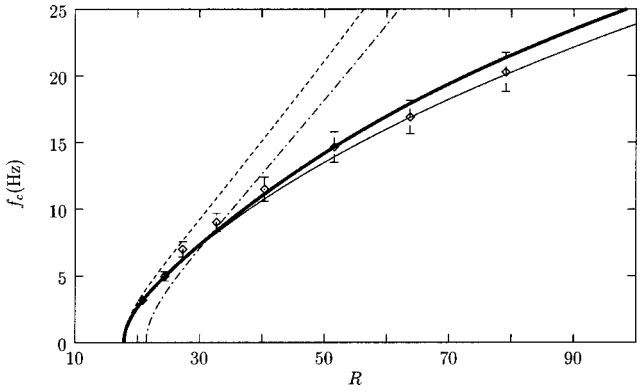

FIG. 1. Cut-off frequency f_c as a function of the Reynolds number R in the conditions of Liu *et al.* (Ref. 18) (glycerin-water mixture, $\beta=4°$, $\Gamma=2341$). Experimental results (diamonds) compared to predictions from Shkadov's model (dot–dashed), first-order model (dashed), simplified second-order model (thin solid), and full second-order model (thick solid).

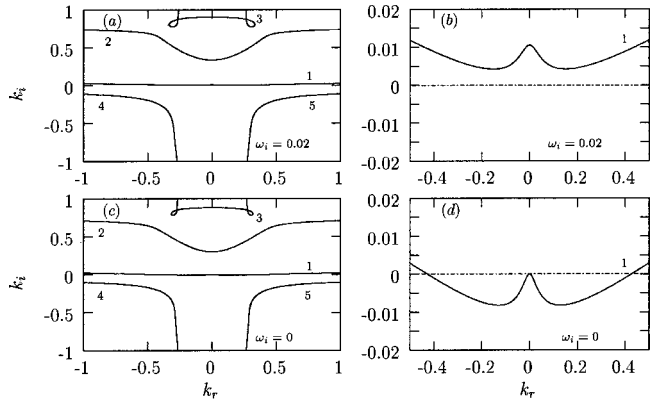

FIG. 2. Spatial branches k_n in the (k_r, k_i) plane for dispersion relation (19) with $\omega_i=0.02$ (top) and $\omega_i=0.0$ (bottom). $R=40$, $\beta=4.6°$, $W=41.46$ ($\Gamma=769.8$). Left: overall view of the diagram. Right: zoom on the neighborhood of the origin in the complex k plane.

change,[16] in agreement with Chang's conjecture.[2] Notice that, in Fig. 1, the cut-off frequency is given in physical units (Hz), whereas the implicit time scale in the dispersion relations and their consequences, especially (17), is $h_N/u_N = 2/h_N$. At large Reynolds number and fixed Kapitza number, $R/W \sim h_N^5 \sim R^{5/3}$ so that the estimation (17) yields an asymptotic behavior of f_c in $R^{7/6}$ for the two first-order models, hence a seemingly linear behavior for the corresponding curves.

A more sensitive check of the accuracy of the models can be obtained from the study of the linear dynamics of wave packets, for which exact numerical results of Brevdo *et al.*,[12] obtained using the full linearized Navier–Stokes equations, are available. As is well known,[19] $D(k,\omega)=0$ being the formal expression of the dispersion relation, the asymptotic behavior of an infinitesimal perturbation initiated at position $x=0$ and time $t=0$, as observed at the limit $t \to \infty$ in a frame moving at speed V with respect to the laboratory (i.e., $x=Vt$), is determined by the root in $k \in \mathbb{C}$ of the system $D(k,\omega+Vk)=0$ and $\partial_k D(k,\omega+Vk)=0$ which has the largest imaginary part ω_i and further satisfies a so-called "collision criterium."[20] This criterium, which follows from causality (film uniformly flat for any $t<0$), states that, in order to be physically relevant, the solution has to arise from the pinching of two spatial branches coming from different sides of the real axis $k_i=0$. Considering the case $V=0$, i.e., in the laboratory frame, the instability is further termed "convective" if the disturbance vanishes on the spot of initiation and "absolute" in the opposite case. In the convective case, the flow behaves as a noise amplifier responding to the upstream disturbances. In the absolute case, the flow behaves as an oscillator having is own dynamics. The convective–absolute nature of the instability can be determined from the sign of the maximum of the ω_i corresponding to the k-roots of $D(k,\omega)=0$ verifying the collision criterium. Comforting experimental evidence, Brevdo *et al.*[12] have shown that the flow over inclined planes is convectively unstable at least up to very large Reynolds numbers and contrary to some model predictions. Here we examine how far our models can reproduce the exact results, restricting our attention to the full second-order model [(3), (11)–(13)] and its simplified version [(3), (14)] since the first-order model [(3), (8)] fails to reproduce the marginal stability conditions correctly due to the neglect of viscous dispersion. Whereas for Navier–Stokes equations, the dispersion relation is obtained from the numerical solution of a differential problem in the cross-stream coordinate, here it is just a polynomial equation in k and ω that can easily be solved (though not explicitly in the case of the full second-order model since it is of degree six in k and, in practice, also in the other case where it is of degree four only).

As done by Brevdo *et al.*, we consider first the case $R=40$, $\Gamma=769.8$, $\beta=4.6°$, corresponding to experiments by Liu *et al.*[21] in order to be able to compare our model predictions with results depicted in Fig. 3 of Ref. 12. Spatial branches in the (k_r, k_i) plane are displayed in Figs. 2 and 3 for dispersion relations (19) and (18), respectively. Their roots in k are computed as ω_r is varied for different values of ω_i. The agreement between results using the full second-order dispersion relation (19) and the exact results is truly remarkable. All the branches observed by Brevdo *et al.*, as well as their change as ω_i is varied from 0.02 (Fig. 2, top) to 0 (bottom), are recovered. Small departures from the exact solutions are only noticeable far from the origin (Fig. 2, left).

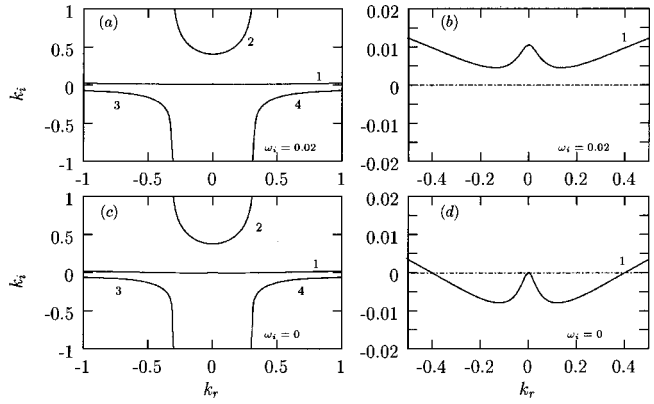

FIG. 3. Spatial branches k_n for dispersion relation (18). Same conditions as in Fig. 2.

TABLE I. Comparison of the saddle point positions between solutions of the dispersion relation of the second-order model, Eq. (19), of the simplified model, Eq. (18) and solutions of the linearized Navier–Stokes problem by Brevdo *et al.* (Ref. 12) ($R=200$, $\beta=4.6°$, and $\Gamma=769.8$).

	Branch	k_r	k_i	ω_r	ω_i
		V=1.15			
Brevdo *et al.*	I	0.17	−0.178	0.0182	0.0062
Eq. (19)	I	0.172	−0.176	0.0182	0.006 27
Brevdo *et al.*	II	0.043	−0.046	0.01	0.0073
Eq. (19)	II	0.040	−0.046	0.0107	0.0073
Eq. (18)		0.0478	−0.0387	0.0099	0.007 25
		V=1.16			
Brevdo *et al.*	I	0.19	−0.165	0.015	0.0079
Eq. (19)	I	0.181	−0.163	0.0165	0.007 96
Brevdo *et al.*	II	0.045	−0.048	0.01	0.0078
Eq. (19)	II	0.0430	−0.0475	0.0103	0.007 77
Eq. (18)		0.0516	−0.0385	0.0098	0.007 64

The agreement turns to excellent when approaching the origin $k=0$ (right), in line with the expectations from the long-wavelength assumption underlying our modeling. Upon decreasing the imaginary part, ω_i, of the frequency from positive to negative values, no pinching of the spatial branches k_n is observed before ω_i becomes negative, which is a clear indication of the convective nature of the instability. Expression (19) may accordingly be seen as an expansion of the true dispersion relation in the limit $k,\omega \ll 1$.

The behavior of the spatial branches corresponding to the simplified second-order dispersion relation (18) is displayed in Fig. 3. The operator D is a polynomial of degree four in k so that all the branches obtained by Brevdo *et al.* cannot be recovered. However, Branch 2 in Fig. 3 clearly seems to result from the hybridization of Branches 2 and 3 in Fig. 2 and the physically most relevant branch, namely Branch 1, is quantitatively close to those obtained using either the full second-order model (Fig. 2) or the primitive equations (Fig. 3 in Ref. 12).

The agreement between model and exact results found for the case $V=0$ extends to the case $V\neq 0$. A detailed account will be the subject of a separate publication. Let us just mention that the full second-order model quantitatively reproduces exact results up to at least $R=200$ in the experimental conditions of Liu and Gollub, including the very peculiar change of dominant saddle-point documented in Ref. 12, see Table I.[22] The simplified model turns out to remain accurate only up to about $R=100$, an already respectable value. As a matter of fact, beyond $R=100$ the latter model does not succeed in reproducing the two branches. However, it seems to interpolate smoothly between them, predicting the total V-width of the unstable band and all other characteristics of the instability (ω_r, ω_i, k_r, k_i) satisfactorily as a function of V. The reason of this semisuccess lies in the fact that, while the function basis used in the Galerkin method is not large enough to fully account for the flow properties, a projection on its first element only already contains most of the physics at a near-quantitative level.

We end this section by considering the spatial stability problem ($\omega\in\mathbb{R}$, $k\in\mathbb{C}$). The spatial growth rate $-k_i$ and the wave number k_r are displayed for the second-order model and the simplified model as a function of the signalling pulsation ω in Figs. 4 and 5, respectively. The results obtained in a wide range of Reynolds numbers using the second-order order model are again in excellent agreement with those obtained by Brevdo *et al.*, whereas the simplified model predicts growth rates somewhat too small at large Reynolds

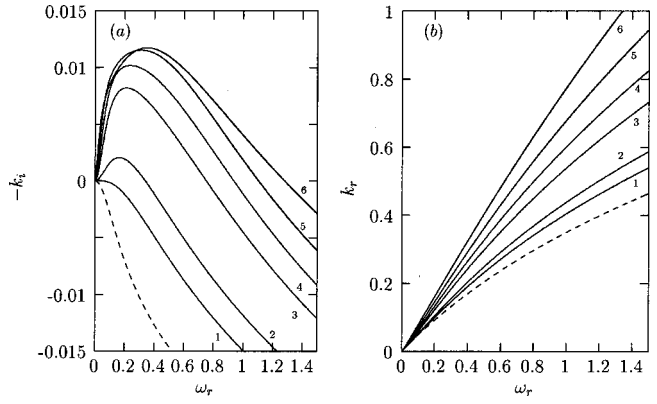

FIG. 4. (a) Growth rate $-k_i$ and (b) wave number k_r of spatially amplified waves as functions of signalling frequency ω_r for the full second-order model. $\Gamma=769.8$, $\beta=4.6°$, $R=10$ (dotted), $R=R_c$ (Curve 1), $R=20$ (2), $R=40$ (3), $R=60$ (4), $R=100$ (5), $R=200$ (6).

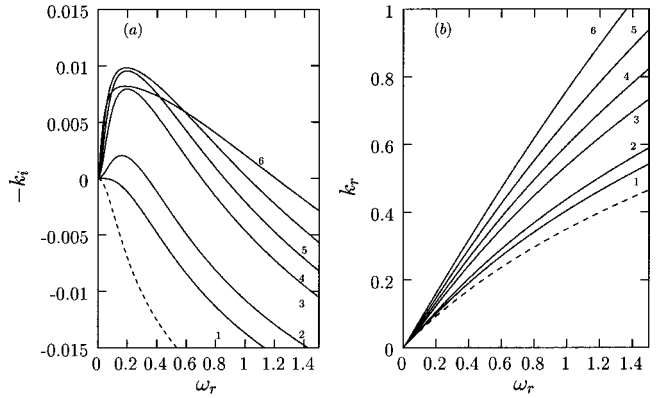

FIG. 5. (a) Growth rate $-k_i$ and (b) wave number k_r of spatially amplified waves as functions of signalling frequency ω_r for the simplified model. Parameters as in Fig. 4.

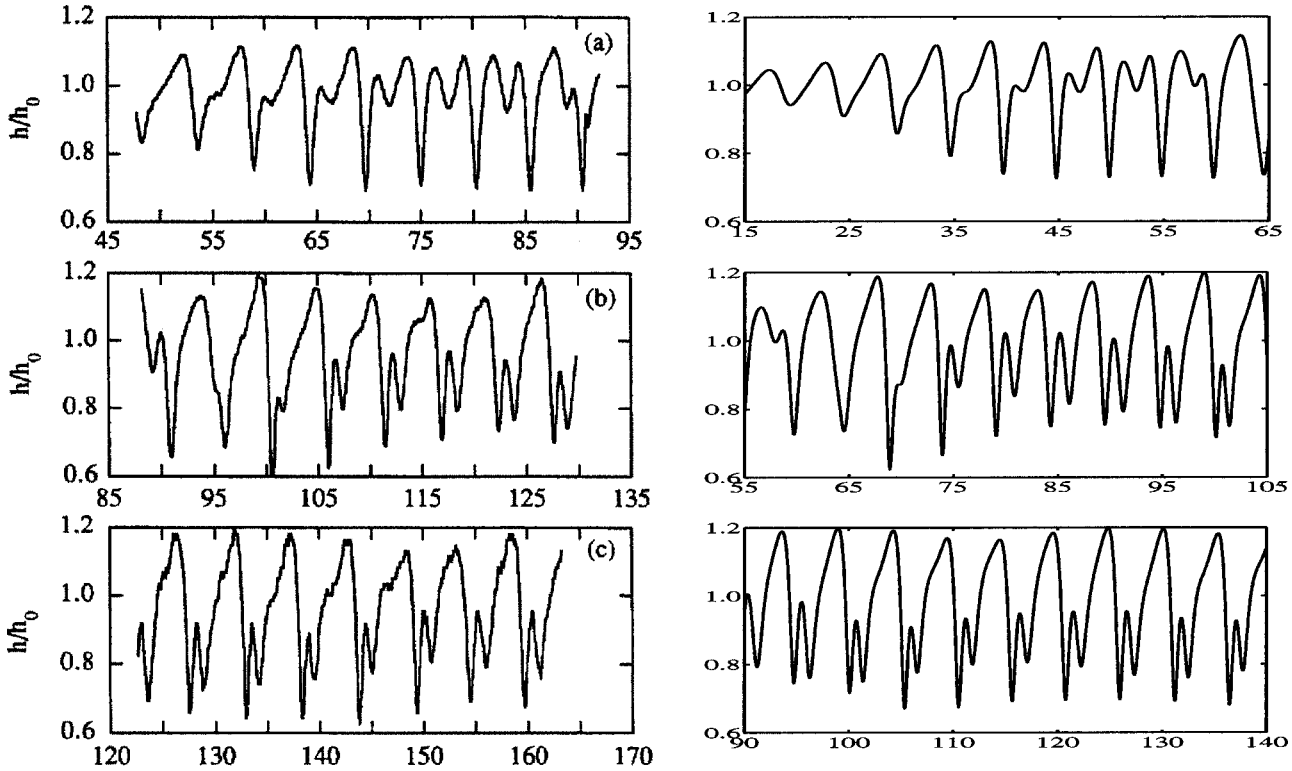

FIG. 6. Experiments (left) and simulation of the simplified model (right) in the experimental conditions of Liu and Gollub (Ref. 13) (glycerin-water mixture, $\beta=6.4°$, $R=29$, $\Gamma=524.4$). Snapshots of the film thickness at three different locations from upstream (top) to downstream (bottom) at forcing frequency $f=4.5$ Hz and forcing amplitude $A=0.03$.

number ($R=100$ and $R=200$), though continuing to predict the wave vector correctly. Agreement with exact results is of course lost for both models when R is set to very high values. For example at $R=4100$, $\beta=4°$, and $W=1.983$ the predicted range of unstable signalling frequency is 25–30 times wider than that obtained by Brevdo *et al.*, but we cannot expect that the assumptions made to derive the models are still valid in such ranges of parameters.

IV. NONLINEAR DYNAMICS OF A PERIODICALLY FORCED FILM

We now turn to numerical simulations results relative to model [(3), (14)] in the nonlinear regime beyond threshold, aiming at a semiquantitative comparison with the experiments performed by Liu and Gollub[13] and the direct numerical simulations of Ramaswamy *et al.*[14]

Depending on the forcing frequency f, laboratory experiments[13] as well as simulations[14] have revealed two different kinds of two-dimensional film evolution (without modulations in the spanwise direction z). In the high-frequency regime, downward the initial exponential growth domain, the waves saturated through a complicated nonlinear process and trains of multipeaked waves were observed. In the low-frequency regime, the exponential growth was directly followed by the formation of trains of solitary-like waves.

A second-order finite-difference quasi-linearized Crank–Nicholson scheme[23] has been implemented to study the nonlinear response of the film submitted to a periodic forcing. A simplified version of the downstream free-boundary condition has been used in order to keep a banded matrix of constant width. The so-introduced numerical inaccuracy turned out to remain confined to a small downstream boundary layer that never grew upstream, owing to the convective nature of the instability. The flow rate at the entrance has been modulated according to

$$q(0,t)=q_N[1+A\cos(2\pi ft)], \tag{20}$$

in line with experiments in Ref. 13 in which sinusoidal perturbations were applied to the film *via* the pressure manifold at the inlet. Parameters corresponding to the same experimental conditions have been chosen, namely $R=29$, $\Gamma=524.4$, and $\beta=6.4°$.

The results of our simulations for $f=4.5$ Hz and $f=1.5$ Hz are compared to experimental snapshots of the film thickness in Figs. 6 and 7. Because the length of the exponential growth region depends on the forcing amplitude, we have chosen to set it arbitrarily to $A=0.03$ and to compare the waves at corresponding amplitude levels rather than at corresponding distances from the inlet. In the high-frequency regime at $f=4.5$ Hz, the simplified model seems to reproduce the nonlinear multipeaked wave evolution reported in the experiment quite faithfully. In particular, the growth of a secondary peak, the phase locking that follows, and the modulation of the waves are all recovered. The length, amplitude, and shape of the waves obtained sufficiently far downstream are in very good agreement with their experimental counterparts. At lower frequency, $f=1.5$ Hz, though

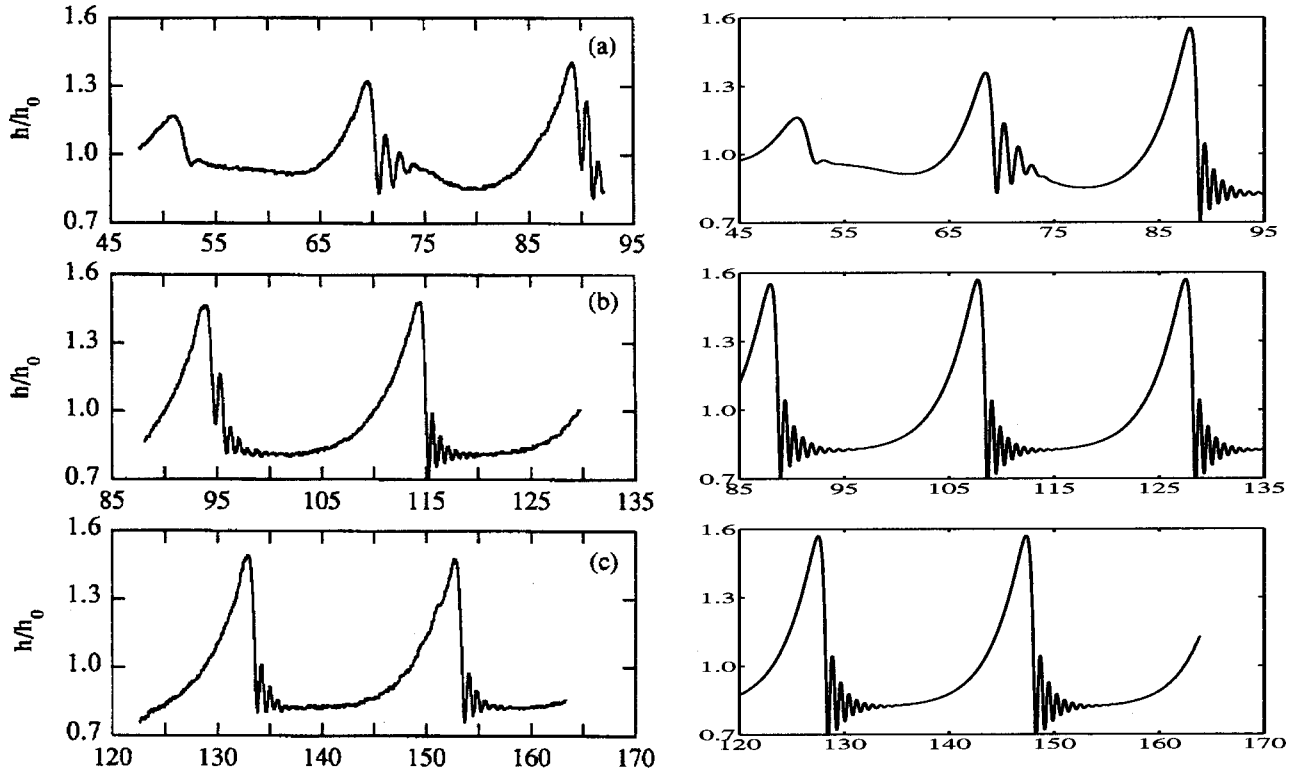

FIG. 7. Experiments (left) and simulation of the simplified model (right) for $f=1.5$ Hz. Other parameters as in Fig. 6.

the direct nonlinear evolution to solitary wavetrains is recovered, the simplified model predicts a wave of slightly larger amplitude than in experiments. The amplitude of the ripples preceding the main hump also seems to be overestimated. These features, already observed with our earlier models,[16] can also be noted in the direct numerical simulations performed by Ramaswamy *et al.*,[14] which suggests that, in fact, the phase-sensitive averaging technique used in experiments could have somehow smoothed the wave profiles and partly erased their steepest parts.

Comparison has also been attempted with direct numerical simulations provided by Ramaswamy *et al.* The spatiotemporal diagrams corresponding to Figs. 14 and 16 in Ref. 14 are presented in Fig. 8. At low frequency, in the solitary-like wavetrain regime, the steepening of the initially sinusoidal waves is followed by the development of ripples in front of each saturated main hump. The front wave is seen to move faster and to have a larger size than its followers. Both of these features have been observed by Ramaswamy *et al.* who force on the film thickness h rather than on the flow rate q as done here. The amplitude was set to $A=0.15$ for the simulation shown in Fig. 8 (left column) which reproduces results displayed in Fig. 14 of Ref. 14 rather closely. Different amplitudes have been tried and, though the transient evolution of the first front is different, the final regime is not modified except for the length of the exponential growth region which is longer for smaller forcing amplitudes. We may, therefore, conclude that the direct formation of solitary waves at low frequency is robust and does not depend on the amplitude of the forcing, or the way it is applied.

At larger frequency, in the multipeaked wave regime, like in laboratory experiments,[13] the nonlinear evolution of the film is complicated and three main regions can be identified, corresponding to the initial exponential growth, the formation of the multipeaked waves, and the final wavetrain modulation. Results displayed Fig. 8 (right column), obtained with a forcing amplitude $A=0.03$, are quite similar to those presented by Ramaswamy *et al.* in their Fig. 16. Even the radiation of a hole-like pulse by the leading front wave visible in the direct numerical simulation can be observed here. Modulations of the saturated wavetrains are, however, somewhat smaller here than in Ref. 14, an observation that does not seem to be changed by varying the forcing amplitude A.

V. COMPARISON OF WEIGHTED RESIDUAL TECHNIQUES

Let us now turn to the convergence properties of weighted-residual methods applied to film flow modeling. It has been shown by a detailed algebraic argument[7] that increasing the level of truncation of any weighted-residual method based on polynomial test functions always lead to the same ''optimal'' system of equations, (3) and (8) at first order in ϵ and (3), (11)–(13) at second order in ϵ. Convergence towards the first-order optimal model was further studied in Ref. 24, in which it was shown that the standard Galerkin method (weight functions identical to basis functions) was the most efficient one, in producing (8) already at level 0. The study of convergence towards the full second-order model, in addition to being very cumbersome, would probably not be much illuminating since that model involves

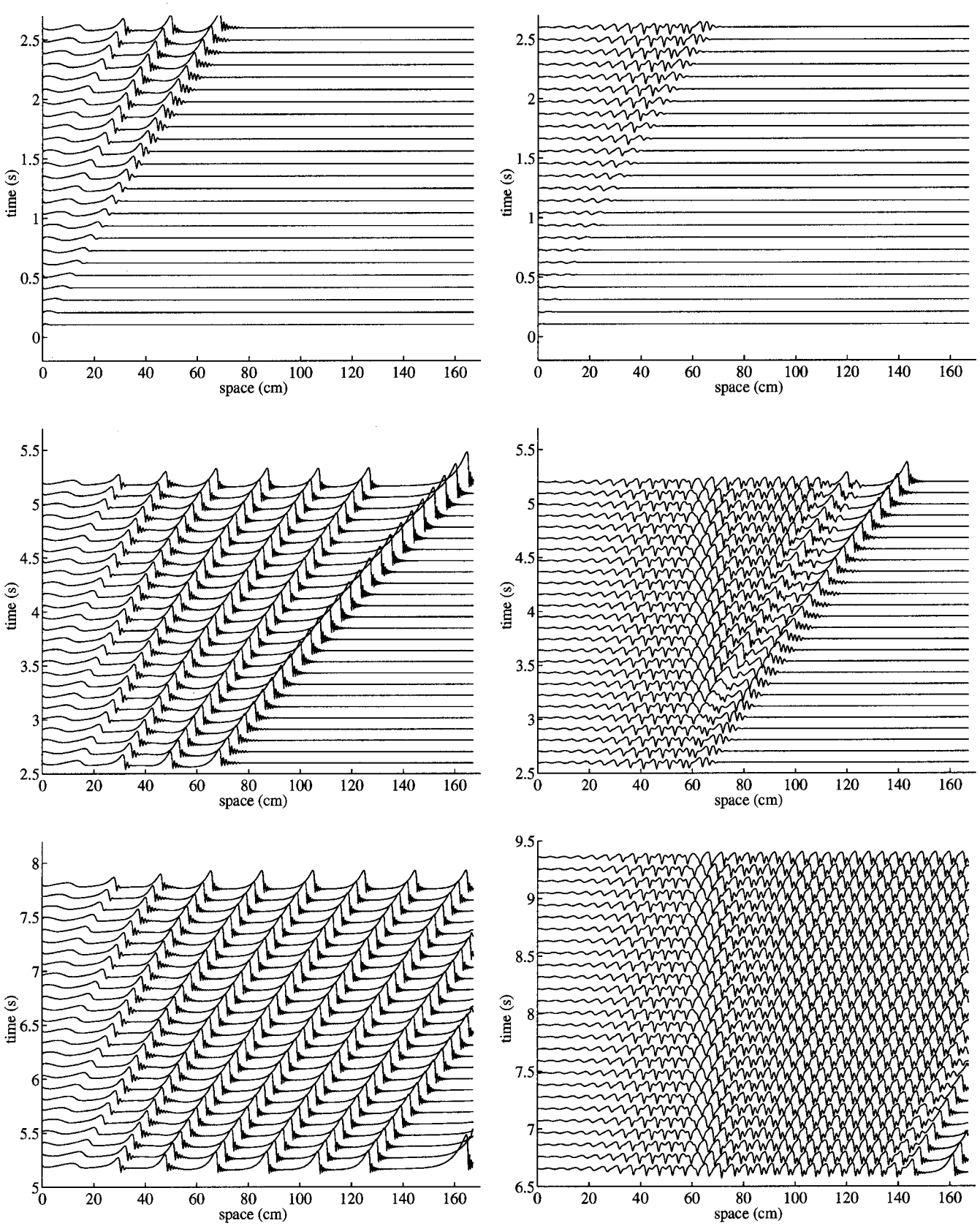

FIG. 8. Film thickness evolution in the experimental conditions of Liu and Gollub (Ref. 13). Left: $f=1.5$ Hz, $A=0.15$. Right: $f=4.5$ Hz, $A=0.03$. For comparison with Figs. 14 and 16 in Ref. 14, respectively.

TABLE II. Method of subdomains.

$j_{\max}$	κ_1	κ_2	κ_3	κ_4	κ_5	κ_6	κ_7
0	$\frac{6}{5}=1.2$	$\frac{12}{5}\frac{7}{17}\simeq 0.988$	$\frac{6}{5}\frac{7}{9}=0.933$	$9\frac{1}{4}=2.25$	$9\frac{2}{9}=2$	$\frac{9}{2}\frac{1}{6}=0.75$	$\frac{7}{2}\frac{2}{9}\simeq 0.778$
1	$\frac{6}{5}=1.2$	$\frac{12}{5}\frac{7}{17}\simeq 0.988$	$\frac{6}{5}\frac{7}{9}=0.933$	$\frac{9}{2}\frac{1}{4}=1.125$	1	$\frac{27}{4}\frac{1}{6}=1.125$	$5\frac{2}{9}\simeq 1.11$
2	$\frac{16}{19}\frac{6}{5}=1.01$	$\frac{1851}{760}\frac{7}{17}\simeq 1.003$	$\frac{993}{760}\frac{7}{9}\simeq 1.02$	$\frac{72}{19}\frac{1}{4}\simeq 0.947$	$\frac{84}{19}\frac{2}{9}\simeq 0.982$	1	$\frac{86}{19}\frac{2}{9}\simeq 1.006$
3	1	$\frac{175}{72}\frac{7}{17}\simeq 1.0008$	$\frac{31}{24}\frac{7}{9}\simeq 1.004$	1	1	1	1
4	1	$\frac{2487}{1024}\frac{7}{17}\simeq 1.00\,006$	$\frac{1317}{1024}\frac{7}{9}\simeq 1.0003$	1	1	1	1
5	1	1	1	1	1	1	1

three equations with many coefficients. Here we rather consider the slightly different, but still instructive, problem of convergence towards the second-order simplified model (14). In order to obtain this model, a supplementary adiabatic elimination step has to be performed, which comes to the neglect of inertia terms in the momentum equation everytime they are second-order in the long-wavelength expansion. So, to be rigorous, convergence of the weighted-residual approach to the film flow problem is studied in this restricted context, which is however easy to implement at each approximation levels.

An appropriate set of basis functions is

$$f_0=\overline{y}-\tfrac{1}{2}\overline{y^2},\ f_j=\overline{y^{j+1}},\ 1\leqslant j\leqslant j_{\max}, \tag{21}$$

so that f_0 corresponds to the flat film velocity profile and other functions verifies the no-slip boundary condition (6) from the start $[f_j(0)=0]$. When truncated above $j_{\max}\geqslant 1$ this set forms a complete basis for polynomials of degree up to $j_{\max}+1$ included. Expanding the streamwise velocity we write

$$u=\sum_{j=0}^{j_{\max}} a_j(x,t) f_j(\overline{y}), \tag{22}$$

where amplitude a_0 is of order unity, amplitudes a_j, $1\leqslant j\leqslant j_{\max}$, being smaller, and their first-order time–space derivatives even smaller. The cross-stream velocity v is then evaluated by integrating the continuity equation (4), i.e., $v=-\int_0^y \partial_x u\, dy$. Weight functions $w_{j'}(\overline{y})$ being specified, residuals are obtained by integrating the streamwise momentum equation over the depth

$$\int_0^h w_{j'}(y/h)(\partial_t u+u\partial_x u+v\partial_y u-\partial_{yy}u-2\partial_{xx}u)\,dy$$
$$=(h+h\partial_x[\partial_x u|_h]-Bh\partial_x h+\Gamma h\partial_{xxx}h)\int_0^1 w_{j'}(\overline{y})\,d\overline{y}. \tag{23}$$

The continuity of the tangential stress at the free surface, expressed by (10), is a nontrivial condition which, in general, cannot be fulfilled at second order as long as the set of test functions is reduced to its first element f_0 since $\partial_{\overline{y}} f_0|_1=0$. By contrast, constraint (10) can be implemented as soon as $j_{\max}\geqslant 1$. At such an approximation level, we have $j_{\max}+1$ unknown amplitudes a_j, for which we need $j_{\max}+1$ equations, hence $j_{\max}$ independent conditions of the form (23) in addition to that issued from (10). Neglecting inertia at second order comes to setting derivatives of amplitudes a_j, $1\leqslant j\leqslant j_{\max}$, strictly to zero in these equations, which leaves us with a system that can be solved for them, and from which an equation for q is finally derived.

As discussed in Sec. II, whatever the weighting strategies and the approximation levels, the equation expressing momentum conservation in all two-equation models for h and q obtained in this way always has the same structure as (14) and can be specified by the coefficients in factor of each term. Comparison between approximation levels can thus be made on the basis of coefficients κ_i defined by writing it in the form

$$\partial_t q=\frac{5}{6}\kappa_1\left(h-Bh\partial_x h+\Gamma h\partial_{xxx}h-3\frac{q}{h^2}\right)-\frac{17}{7}\kappa_2\frac{q}{h}\partial_x q$$
$$+\frac{9}{7}\kappa_3\frac{q^2}{h^2}\partial_x h+4\kappa_4\frac{q}{h^2}(\partial_x h)^2-\frac{9}{2h}\kappa_5 q\partial_x q\partial_x h$$
$$-6\kappa_6\frac{q}{h}\partial_{xx}h+\frac{9}{2}\kappa_7\partial_{xx}q, \tag{24}$$

and studying the convergence of the coefficients κ_i so introduced towards 1 as the truncation level increases. For example, the ability of a given model to capture the instability mechanism can be appreciated from κ_1 that turns out to measure the ratio of the linear threshold to the exact theoretical

TABLE III. Collocation method.

$j_{\max}$	κ_1	κ_2	κ_3	κ_4	κ_5	κ_6	κ_7
0	$\frac{8}{9}\frac{6}{5}\simeq 1.07$	$\frac{19}{8}\frac{7}{17}\simeq 0.978$	$\frac{9}{8}\frac{7}{9}=0.875$	$\frac{32}{3}\frac{1}{4}\simeq 2.67$	$\frac{28}{3}\frac{2}{9}\simeq 2.07$	$\frac{14}{3}\frac{1}{6}\simeq 0.778$	$\frac{10}{3}\frac{2}{9}\simeq 0.741$
1	$\frac{8}{9}\frac{6}{5}\simeq 1.07$	$\frac{19}{8}\frac{7}{17}\simeq 0.978$	$\frac{9}{8}\frac{7}{9}=0.875$	$\frac{20}{3}\frac{1}{4}\simeq 1.67$	$\frac{16}{3}\frac{2}{9}\simeq 1.19$	$\frac{20}{3}\frac{1}{6}\simeq 1.11$	$\frac{14}{3}\frac{2}{9}\simeq 1.04$
2	$\frac{48}{61}\frac{6}{5}\simeq 0.944$	$\frac{2669}{1098}\frac{7}{17}\simeq 1.0009$	$\frac{473}{366}\frac{7}{9}\simeq 1.005$	$\frac{312}{61}\frac{1}{4}\simeq 1.28$	$\frac{300}{61}\frac{2}{9}\simeq 1.09$	1	$\frac{266}{61}\frac{2}{9}\simeq 0.969$
3	1	$\frac{2497}{1024}\frac{7}{17}\simeq 1.004$	$\frac{1347}{1024}\frac{7}{9}\simeq 1.02$	1	1	1	1
4	1	1	1	1	1	1	1

TABLE IV. Integral-collocation method.

$j_{\max}$	κ_1	κ_2	κ_3	κ_4	κ_5	κ_6	κ_7
0	$\frac{6}{5}=1.2$	$\frac{12}{5}\frac{7}{17}\simeq 0.988$	$\frac{6}{5}\frac{7}{9}\simeq 0.933$	$9\frac{1}{4}=2.25$	$9\frac{2}{9}=2$	$\frac{9}{2}\frac{1}{6}=0.75$	$\frac{7}{2}\frac{2}{9}\simeq 0.778$
1	$\frac{6}{5}=1.2$	$\frac{12}{5}\frac{7}{17}\simeq 0.988$	$\frac{6}{5}\frac{7}{9}\simeq 0.933$	$\frac{9}{2}\frac{1}{4}=1.125$	1	$\frac{27}{4}\frac{1}{6}=1.125$	$5\frac{2}{9}\simeq 1.11$
			(a) Derivatives evaluated at $y=0$				
2	$\frac{8}{11}\frac{6}{5}\simeq 0.87$	$\frac{126}{55}\frac{7}{17}\simeq 0.94$	$\frac{48}{55}\frac{7}{9}\simeq 0.68$	$\frac{72}{11}\frac{1}{4}\simeq 1.64$	$\frac{60}{11}\frac{2}{9}\simeq 1.21$	1	$\frac{46}{11}\frac{2}{9}\simeq 0.929$
3	1	$\frac{21}{8}\frac{7}{17}\simeq 1.08$	$\frac{15}{8}\frac{7}{9}\simeq 1.46$	1	1	1	1
4	1	$\frac{19}{8}\frac{7}{17}\simeq 0.978$	$\frac{9}{8}\frac{7}{9}\simeq 0.875$	1	1	1	1
5	1	1	1	1	1	1	1
			(b) Derivatives evaluated at $y=h$				
2	1	$2\frac{7}{17}\simeq 0.824$	$1\frac{7}{9}\simeq 0.778$	0	$\frac{5}{2}\frac{2}{9}\simeq 0.556$	$5\frac{1}{6}\simeq 0.833$	$\frac{25}{6}\frac{2}{9}\simeq 0.926$
3 & 4	1	$\frac{5}{2}\frac{7}{17}\simeq 1.03$	$\frac{3}{2}\frac{7}{9}\simeq 1.17$	1	1	1	1
	1	1	1	1	1	1	1

value, $\kappa_1=q_c/q_c^{(\mathrm{th})}$. Other coefficients would affect nonlinear predictions such as the amplitude and speed of nonlinear solitary waves beyond threshold.

A. Method of subdomains

This is a generalization of the integral method leading to Shkadov's model: Integrating the momentum equation over the depth using just f_0 and a uniform weight, and neglecting terms formally of order ϵ^2 (coefficients $\kappa_{4,5,6,7}\equiv 0$) indeed yields (2). For $j_{\max}=1$, the condition emanating from (10) is added to the same integrated equation. For $j_{\max}>1$, the $\overline{y}$-interval [0,1] is cut into $j_{\max}$ equal adjacent subintervals by $j_{\max}-1$ (e.g., equally distributed) break points. The velocity profile u is expanded onto the first $j_{\max}+1$ basis functions in (21) and further inserted into (9) which is integrated over each of these subintervals. The resulting linear system for the a_j is then solved as sketched above. Corresponding coefficients κ_i appearing in (24) are given in Table II.[25] Linear properties are recovered for $j_{\max}=3$ ($\kappa_1=1$). Convergence is nearly achieved already for $j_{\max}=3$ but $j_{\max}=5$ is necessary for complete nonlinear agreement.

B. Collocation method

The weight functions w_j are now δ-functions peaked at specific points in the interval [0,1]. The cancellation of residuals correspond to the exact fulfillment of the equation at those locations. When $j_{\max}=0$, the residual corresponds to the evaluation of (9) at $\overline{y}=1/2$. Otherwise, boundary condition (10) is completed by computing the residual at $j_{\max}$ equally spaced collocation points, which results in Eq. (24) with coefficients given in Table III. Full convergence is observed at level $j_{\max}=4$.

C. Integral-collocation method

In this method, a simple averaging of Eq. (9) is supplemented by additional conditions generally placed at the boundaries. As an example, we test here the conditions chosen in Ref. 16, namely

$$\partial_{y^k}(\partial_t u+u\partial_x u+v\partial_y u-\partial_{yy}u-2\partial_{xx}u)=0, \quad \text{at} \quad y=0. \tag{25}$$

Shkadov's integral method is recovered at level 0. Boundary condition (10) is added at level 1 while at higher levels the set of residuals is completed by (25) for $k=1,\ldots,j_{\max}-1$. Results are given in Table IV(a). Those corresponding to the same conditions but evaluated at the interface $y=h$ are given as (b) in the same table. In spite of our expectations, the integral-collocation method initially developed in Ref. 16 has thus pretty poor convergence properties, especially when the additional collocation conditions are situated at the plane. The situation is slightly better when they are set at the interface, which might be related to the fact that the instability mechanism involves processes that take place at the interface (energy transfer in the bulk flow through the work of the shear at the interface[26]).

D. Method of moments

The weights used at the projection step are monomials of increasing degree $w_k=\overline{y^k}$. The equation is fulfilled "in probability" by canceling its successive moments. Level 0, with $w_0\equiv 1$ again corresponds to simple averaging, thus leading to Shkadov's model, coefficients $\kappa_{1,2,3}$, plus some second order terms involving coefficients $\kappa_{4,5,6,7}$. As far as $\kappa_{1,2,3}$ are concerned, at level 1 using f_0 and f_1 as test functions yields the same result. The convergence of the method is rather fast, as seen from results collected in Table V.

TABLE V. Method of moments.

$j_{\max}$	κ_1	κ_2	κ_3	κ_4	κ_5	κ_6	κ_7
0	$\frac{6}{5}=1.2$	$\frac{12}{5}\frac{7}{17}\simeq 0.988$	$\frac{6}{5}\frac{7}{9}=0.933$	$9\frac{1}{4}=2.25$	$9\frac{2}{9}=2$	$\frac{9}{2}\frac{1}{6}=0.75$	$\frac{7}{2}\frac{2}{9}\simeq 0.778$
1	$\frac{6}{5}=1.2$	$\frac{12}{5}\frac{7}{17}\simeq 0.988$	$\frac{6}{5}\frac{7}{9}=0.933$	$\frac{9}{2}\frac{1}{4}=1.125$	1	$\frac{27}{4}\frac{1}{6}=1.125$	$5\frac{2}{9}\simeq 1.11$
2	$\frac{16}{19}\frac{6}{5}\simeq 1.01$	$\frac{231}{95}\frac{7}{17}\simeq 1.001$	$\frac{123}{95}\frac{7}{9}\simeq 1.007$	$\frac{72}{19}\frac{1}{4}\simeq 0.947$	$\frac{84}{19}\frac{2}{9}\simeq 0.982$	1	$\frac{86}{19}\frac{2}{9}\simeq 1.006$
3	1	1	1	1	1	1	1

E. Galerkin method

The test functions themselves are now taken as weight functions, $w_j \equiv f_j$. As shown in Ref. 7, the simplified second-order model is obtained already at level 0. This fast convergence property is not a miracle but can be understood from the consideration of (5). Indeed, its left-hand side (l.h.s.) of order unity and its right-hand side (r.h.s.) is formally small. Therefore, the variables $a_i(x,t)$, $i \geqslant 1$, themselves small, can appear in the residuals $\mathcal{R}_j$ only through the integrals $\int_0^h w_j(\bar{y}) \partial_{yy} u \, dy$ on the l.h.s. of (5). For $j=0$, an integration by part making use of (10) at $y=h$ directly leads to

$$\int_0^h f_0(y/h) \partial_{yy} u \, dy = -\frac{q}{h^2}, \tag{26}$$

which involves q and not the a_j separately. The formulation is thus already closed at this stage, which brings the result.

F. Remarks

When looking at the tables, one observes that the variations of the coefficients are not monotonic as the approximation level is increased, and that the limit can be reached ''from above'' as well as ''from below,'' which is not surprising since the full problem has no underlying variational structure.[11] More interestingly, the sub-domain method and the collocation method are seen to display similarly slow convergence properties, a fact to be put in relation with their ''finite-difference'' type of approximation. By contrast, the method of moments and the Galerkin method converge faster owing to their ''spectral'' flavor. The latter, involving basis functions well adapted to the problem, turns out to be the most efficient.

VI. CONCLUSION

In this paper, we first reviewed our approach to the modeling of fluid films flowing along inclined planes using weighted-residual methods combined to a long-wavelength expansion.[7,16] Let us first list some criteria that, in our opinion, should be met by a useful model, being understood that it must be much easier to study than the primitive free-surface Navier–Stokes equations. These are: (i) An accurate prediction of the linear instability properties, to begin with the threshold (coefficient $\kappa_1 = 1$ in the tables), (ii) the existence of solutions sufficiently far from threshold, ideally for all the range of Reynolds numbers for which the approach resting on the long-wavelength expansion is reasonable, and (iii) a quantitative restitution of the properties of the periodic and solitary waves (speed, amplitude, bifurcation diagram). In this respect, Shkadov's model improves over one-equation models such as the Benney equation only with respect to the occurrence of finite-time singularities beyond threshold,[5] but is not accurate enough as far as linear and nonlinear quantitative properties are concerned. Our first-order model clearly improves over Shkadov's model[8] by correcting its behavior close to threshold but rapidly reveals insufficient as the Reynolds number is increased.

As early noticed by Chang,[2] viscous dispersion is expected to play a significant role at a quantitative level. Consistency at first order in the long-wavelength expansion is insufficient to takes this into account, which calls for our optimal second-order model.[7] The latter involves two slowly varying fields in addition to h and q, hence four equations (3), (11)–(13). It apparently contains all what is needed to fit exact linear properties at least up to $R=200$ in the experimental conditions of Liu *et al.*,[13,18,21] as seen from the comparison with the wave packet analysis of Brevdo *et al.*[12] Since its nonlinear properties were also found satisfactory,[7] it is certainly the best possible choice. It is however somewhat difficult to handle,[24] which gives all its interest to the simplification made by adiabatically eliminating the two additional fields necessary to have full consistence at second order.[27] The remaining model [(3), (14)], which includes viscous dispersion but neglects second-order inertia effects, turns out to give reliable results up to more than $R=100$ in the same experimental conditions, and thus can be a good choice for a semiquantitative exploration of a large range of control parameters ($B=\cot\beta$, film thickness h_N and Kapitza number Γ or Reynolds number R and Weber number W). Now, the disposal of effective models helps us tracing back the deficiencies of some previous attempts[8–10,17] to a lack of flexibility of the velocity profile, to an inappropriate account of viscous dispersion effects or to the introduction of higher order terms that turn out to be inessential.

Finally, it happens that the simplified model can be obtained by applying a genuine Galerkin method to the momentum equation (5) with a single test function f_0. Up to now we have considered streamwise modulations only (the so-called two-dimensional case). The extension of the simplified model to three dimensions, thus involving also spanwise perturbations, is straightforward.[7,24] It should share the same interesting properties and will be the subject of future study.

When compared to other flows, thin films display interesting specificities. First, slow space–time interface modulations develop in a super-critical context and are well described by simplified formulations resting on low orders of a systematic long-wavelength expansion of the primitive equations. Next, the basic flow profile is simply parabolic and polynomial functions form a closed set with respect to differentiation and nonlinear couplings. These circumstances make it easier to build models by means of weighted-residual methods with a well controlled level of accuracy. The ambition of modeling is often to obtain qualitative and not quantitative results, especially when the structure of the model is forced by phenomenological considerations while some freedom is left for the values of its parameters. Our study suggests that optimal parameter sets yielding truly quantitative results can be determined without much additional effort by an appropriate choice of weighted-residual methods taking into account the specificities of the problem at hand. We believe that it might be interesting to follow a similar approach in less well suited cases, especially in subcritical cases such as plane Poiseuille or Couette flow, as an alternative to direct numerical simulations.

ACKNOWLEDGMENTS

This work has been supported by a grant from the French Ministry of Defense (Délégation Générale à l'Armement). The discussion in Sec. III was prompted by the remarks of the anonymous referees regarding a first version of the paper.

[1]P. L. Kapitza and S. P. Kapitza, "Wave flow of thin layers of a viscous fluid," Zh. Eksp. Teor. Fiz. **19**, 105 (1949); also in *Collected Papers of P. L. Kapitza*, edited by D. Ter Haar (Pergamon, Oxford, 1965), pp. 690–709.

[2]H. C. Chang, "Wave evolution on a falling film," Annu. Rev. Fluid Mech. **26**, 103 (1994).

[3]C.-S. Yih, "Stability of two-dimensional parallel flows for three-dimensional disturbances," Q. Appl. Math. **12**, 434 (1955).

[4]D. J. Benney, "Long waves on liquid film," J. Math. Phys. **45**, 150 (1966).

[5]A. Pumir, P. Manneville, and Y. Pomeau, "On solitary waves running down an inclined plane," J. Fluid Mech. **135**, 27 (1983).

[6]T. Ooshida, "Surface equation of falling film flows which is valid even far beyond the criticality," Phys. Fluids **11**, 3247 (1999).

[7]Ch. Ruyer-Quil and P. Manneville, "Improved modeling of flows down inclined planes," Eur. Phys. J. B **15**, 357 (2000).

[8]V. Ya. Shkadov, "Wave flow regimes of a thin layer of viscous fluid subject to gravity," Izv. Akad. Nauk SSSR, Mekh. Zhidk. Gaza **2**, 43 (1967).

[9]J.-J. Lee and C. C. Mei, "Stationary waves on an inclined sheet of viscous fluid at high Reynolds and moderate Weber numbers," J. Fluid Mech. **307**, 191 (1996).

[10]T. Prokopiou, M. Cheng, and H. C. Chang, "Long waves on inclined films at high Reynolds number," J. Fluid Mech. **222**, 665 (1991).

[11]B. A. Finlayson, *The Method of Weighted Residuals and Variational Principles, with Application in Fluid Mechanics, Heat and Mass Transfer* (Academic, New York, 1972).

[12]L. Brevdo, P. Laure, F. Dias, and T. J. Bridges, "Linear pulse structure and signalling in a film flow on an inclined plane," J. Fluid Mech. **396**, 37 (1999).

[13]J. Liu and J. P. Gollub, "Solitary wave dynamics of film flows," Phys. Fluids **6**, 1702 (1994).

[14]B. Ramaswamy, S. Chippada, and S. W. Joo, "A full-scale numerical study of interfacial instabilities in thin-film flows," J. Fluid Mech. **325**, 163 (1996).

[15]S. P. Lin, "Finite amplitude side-band stability of a viscous fluid," J. Fluid Mech. **63**, 417 (1974).

[16]Ch. Ruyer-Quil and P. Manneville, "Modeling film flows down inclined planes," Eur. Phys. J. B **6**, 277 (1998).

[17]This explains that the model recently developed by L. T. Nguyen and V. Balakotaiah ["Modeling and experimental studies of wave evolution on free falling viscous films," Phys. Fluids **12**, 2236 (2000)] does not much better than the integral boundary layer model (Ref. 8). To get rid of the assumption of a similar profile while keeping the idea of a separation of variables, they assumed $u(x,t)=2a(x,t)y+3b(x,t)y^2$ and obtained three coupled equations for h, a, and b. However, inserting this ansatz into the first order tangential stress condition $\partial_y u|_h=0$ decreases the actual number of degrees of freedom by linking a and b through the condition $2a+6bh=0$. Therefore, the velocity profile actually reads $u=2a(y-y^2/(2h))=2ha(\overline{y}-\frac{1}{2}\overline{y^2})$, hence the predicted instability threshold $q_c^{(\mathrm{IBL})}$.

[18]J. Liu, B. Schneider, and J. P. Gollub, "Three-dimensional instabilities of film flows," Phys. Fluids **7**, 55 (1995).

[19]P. Huerre, "Open shear flow instabilities," in *Perspectives in Fluid Dynamics*, edited by G. K. Batchelor, H. K. Moffat, and M. G. Worster (Cambridge University Press, Cambridge, 2000).

[20]A. Bers, "Space–time evolution of plasma instabilities—absolute and convective," in *Handbook of Plasma Physics*, edited by N. M. Rosenbluth and R. Z. Sagdeev (North-Holland, Amsterdam, 1983).

[21]J. Liu, J. D. Paul, and J. P. Gollub, "Measurements of the primary instabilities of film flows," J. Fluid Mech. **250**, 69 (1993).

[22]In the quoted paper, Brevdo *et al.* gives $\omega_r^{\mathrm{II}}=0.015$ for $V=1.16$ in the caption of Fig. 5, which is an obvious misprint as seen from the corresponding curve in their Fig. 7(b).

[23]R. D. Richtmeyer and K. W. Morton, *Difference Methods for Initial Value Problems* (Interscience, New York, 1967).

[24]Ch. Ruyer-Quil, Ph.D. dissertation, École polytechnique, 1999.

[25]The values of coefficients $\kappa_{4,5,6,7}$ prescribed by Prokopiou *et al.* (Ref. 10) are not recovered because the contribution of viscosity to the pressure gradient $\partial_y p$ across the film neglected in that reference are taken into account here.

[26]R. E. Kelly, D. A. Goussis, S. P. Lin, and F. K. Hsu, "The mechanism for surface wave instability in film flow down an inclined plane," Phys. Fluids A **1**, 819 (1989).

[27]Ch. Ruyer-Quil and P. Manneville, "On the introduction of viscous dispersion in the modeling of film flows down inclined planes," Abstract IK3, p. 106, ICTAM2000, 20th International Congress of Theoretical and Applied Mechanics, Chicago, 08/27–09/02/2000.